Catalysis Letters 27 (1994) 207–220

Microkinetic analysis of the oxidative conversion of methane. Dependence of rate constants on the electrical properties of $(CaO)_x(CeO_2)_{1-x}$ catalysts

Dorit Wolf

Lehrstuhl für Technische Chemie, Ruhr-University Bochum, D-44780 Bochum, Germany

Received 1 November 1993; accepted 30 April 1994

Elementary reaction steps of the oxidative conversion of methane to CO_x and ethane were derived from kinetic data for various $(CaO)_x(CeO_2)_{1-x}$ catalysts. The rate constants depend on electron and O^{2-} conductivity as well as on the reducibility of the oxides. It is shown hereby that reactions resulting in increased or in decreased ethane selectivity are interrelated via the same catalyst properties.

Keywords: methane oxidation; microkinetics; CaO–CeO_2 catalysts; electron conductivity; oxygen-anion conductivity

1. Introduction

In the catalytic oxidative conversion of methane primary reactions lead to total oxidation, e.g. CO_x, and to ethane as a coupling product from methyl radicals. The formation of CO_x and C_2H_6 is strongly affected by the catalyst properties, which is reflected by various kinetic models of the primary reaction steps for different catalysts [1–3].

The aim of the present work was to derive a mechanism and the respective rate constants of the various reaction steps for the oxidative conversion of methane using differently composed CaO–CeO_2 catalysts. These catalysts reveal a shift of the product distribution for mainly CO_x production to higher ethane yields with increasing CaO content. Thus, an attempt is made to establish the requirement for either total oxidation or selective coupling by analyzing correlations between the estimated rate constants and solid-state properties of these catalysts.

The suggested mechanistic models included reaction steps on the catalytic surface and in the gas phase. Estimates of the rate constants were obtained by fitting experimental kinetic data of the measurable gas-phase compounds. To observe mainly the effect of the catalyst on the rate of the primary heterogeneous reactions and to confine the complexity of the kinetic model with respect to consecutive

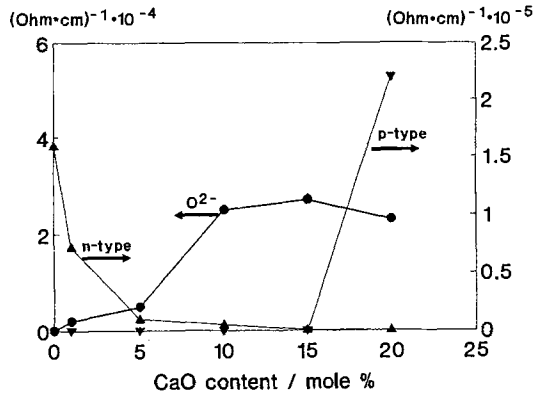

Fig. 1. Oxygen anion conductivity ((●) $T = 1023$ K), electron conductivity n-type ((▲) $p_{O_2} = 3 \times 10^{-2}$ Pa, $T = 1023$ K) and p-type ((▼) $p_{O_2} = 35$ kPa, $T = 1023$ K) as a function of the CaO content in the solid solution $CaO–CeO_2$.

gas-phase reactions experiments were carried out at short contact time (0.012 g s/ml) and low temperatures (< 1000 K).

The rate constants of the best model obtained by discrimination were related to the electron and oxygen-anion conductivity of the $(CaO)_x(CeO_2)_{1-x}$ model catalysts forming solid solutions within the range $0 \leqslant x \leqslant 0.23$ [4]. The incorporation of CaO into the CeO_2 lattice leads to an increase of the oxygen-anion conductivity up to a maximum at about 10–15 mol% CaO [5]. Simultaneously the proportion of n-type conductivity decreases with increasing CaO content while above 15 mol% CaO the catalysts reveal p-type conductivity at high oxygen partial pressure [6] (see fig. 1).

2. Experimental

2.1. PREPARATION AND PROPERTIES OF THE CATALYSTS

The Ce–Ca–O catalysts were prepared by thermal decomposition of the metal oxalates which were obtained by coprecipitation from nitrate solutions at pH = 8; ($Ca(NO_3)_2 \cdot 4H_2O$: Riedel de Haen, >99.9%; $Ce(NO_3) \cdot 6H_2O$: Fluka, >99.9%). The oxalates were thermally treated at 1173 K for 8 h.

The crystalline phases have been analyzed by a counter tube diffractometer (Freiberger Präzisionsmechanik) using Cu K_α radiation. Neither broadening of peaks nor additional phase formation (CaO) besides pure CeO_2 was observed within the range of composition investigated.

The surface concentration of Ce and Ca was measured by a Leybold Heraeus LHS 10 spectrometer (Al K_α X-ray source). No significant difference exists between surface and bulk composition:

Ca/(Ce+Ca) (bulk): 0 0.05 0.10 0.20

Ca/(Ce+Ca) (surface): 0.0 0.07 0.12 0.23.

The surface areas were obtained by the BET-1-point method:

Ca/(Ca+Ce): 0 0.05 0.1 0.2;

surface area (m^2/g): 2.0 2.3 1.9 2.0.

Taking into account the reducibility of this method (ca. 10%) no significant change in the surface area occurs by increasing the CaO content.

2.2. KINETIC MEASUREMENTS

The reaction was carried out in a micro catalytic fixed bed reactor of 8 mm inner diameter with a fixed bed of 0.05 g catalyst (particle diameter 0.1–0.2 mm) diluted by 1.0 g of quartz. Kinetic measurements covered the following range of conditions: 5 kPa $\leqslant p_{CH_4} \leqslant$ 50 kPa, 0.3 kPa $\leqslant p_{O_2} \leqslant$ 15 kPa, 933 K $\leqslant T \leqslant$ 993 K, p_{total} = 0.1 MPa (balance N_2); the contact time of the gas was kept constant at $m_{cat}/F_{(STP)}$ = 0.012 g s/ml. The blank conversion of methane amounted to 0.03% and of oxygen to 0.3% at 1013 K applying partial pressure of methane and oxygen of 50 and 5 kPa, respectively. The gas-phase composition was analyzed by on-line gaschromatography. H_2, O_2, N_2, CO, CH_4 and CO_2 were separated by a carbosieve and detected by TCD; hydrocarbons were separated by Porapak Q and detected by FID. Twenty data sets of different inlet oxygen and methane partial pressures were used for each temperature (933, 963, and 993 K) [7].

3. Evaluation of kinetic data

3.1. KINETIC MODELS

The final reaction scheme and the respective kinetic model were selected among ten others (see table 1) by discrimination based on the quality of fit between experimental kinetic data and simulated ones. Different reaction pathways of methane activation, surface reoxidation, consecutive oxidation of methyl radicals and ethane as well of CO_2 adsorption were considered (see reactions j = 1–14 in table 1). To confine the complexity of the numerical parameter estimation various simplifications were introduced. Ethane and ethylene were lumped to C_2 because of the generally low amount of the secondary product C_2H_4 (C_2H_4/C_2H_6(max) = 0.07) due to the short contact time. Also CO and CO_2 are lumped to CO_x (CO/CO_2(max) = 0.11) although the author is conscious of the fact that both CO and CO_2 may be primary products. The reason for postulating the steps of consecutive oxidation of methyl radicals and ethane (j = 8–11) was to explain the maximum in the C_2H_6 partial pressure at reactor outlet depending on the inlet partial pressure

Table 1
Reaction models and their fitness

j	Reaction steps	Reaction model No.										Ref.
		1	2	3	4	5	6	7	8	9	10	
	methane activation											
1	$CH_4 + [O] \rightleftharpoons CH_3 + [OH]$	•	•	•	•	•	•	•	•	•	•	[8–10]
2	$CH_4 + [O_2] \rightarrow CH_3O + [OH]$				•						•	
	surface oxidation											
3	$O_2 + 2[\,] \rightleftharpoons 2[O]$									•		
4	$O_2 + [\,] \rightleftharpoons [O_2]$	•	•	•	•	•	•	•	•		•	[15]
5	$[O_2] + [\,] \rightarrow 2[O]$	•	•	•	•	•	•	•	•		•	[15]
	dehydration											
6	$2[OH] \rightarrow H_2O + [\,] + [O]$	•	•	•	•	•	•	•	•	•	•	[12]
	ethane formation											
7	$2CH_3 \rightarrow C_2H_6$	•	•	•	•	•	•	•	•	•	•	[8,9,13]
	consecutive reactions											
8	$CH_3 + [O] \rightarrow CH_3O + [\,]$	•	•	•	•	•	•	•	•	•		[11,12]
9	$CH_3 + [O_2] \rightarrow CH_3O_2 + [\,]$		•								•	
10	$CH_3 + O_2 \rightarrow CH_3O_2$			•								[14]
11	$C_2H_6 + [O_2] \rightarrow 2CH_3O + [\,]$					•	•	•	•			[16]
	CO_2 adsorption											
12	$CO_2 + [O] \rightleftharpoons [O]\text{–}CO_2$						•					
13	$CO_2 + 2[O] \rightleftharpoons [O]_2{=}CO_2$							•				
14	$CO_2 + [\,] + [O] \rightleftharpoons [O_2]{=}CO$								•			
	average relative error between experimental and predicted data (%)	14	30	28	12	8	8	8	8	50	50	

of oxygen experimentally observed for catalysts containing CaO (see fig. 2). It should be noted that reaction $j = 11$ has not to be a single elementary step. However, its further subdivision is irrelevant for the fitting procedure.

3.2. PARAMETER ESTIMATION

In the present work rate equations were based on the assumption of steady state of the surface intermediates Θ_i (units of rate constants see list of symbols and fig. 4):

$$\frac{d\Theta_{[O]}}{dt} = \frac{d\Theta_{[O_2]}}{dt} = \frac{d\Theta_{[OH]}}{dt} = \frac{d\Theta_{[\,]}}{dt} = \frac{d\Theta_{[CO_x]}}{dt} = p_{\text{total}}^{-1}\rho_{\text{bed}} \sum_{j=1}^{14} m_{ij} r_j = 0\,, \qquad (1)$$

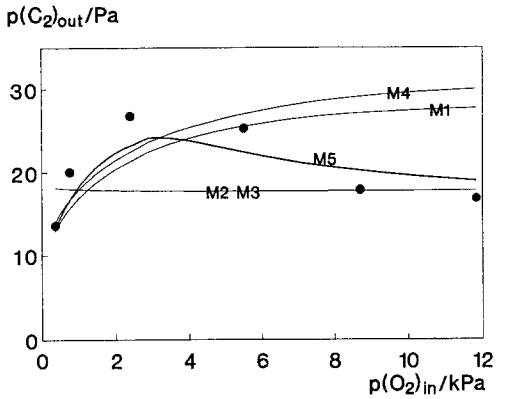

Fig. 2. C_2 outlet partial pressure as a function of the O_2 inlet partial pressure. (—) Fits of different models (10 mol% CaO/CeO_2; $T = 933$ K).

$$1 = \Theta_{[O]} + \Theta_{[O_2]} + \Theta_{[OH]} + \Theta_{[\,]} + m_j \Theta_{[CO_x]}$$

$$(m_j = 1 \text{ if } j = 12; m_j = 2 \text{ if } j = 13; 14)\,. \tag{2}$$

A pseudo-steady state has been assumed for the gas-phase intermediates CH_3, CH_3O, CH_3O_2:

$$0 = \frac{\mathrm{d}p_{CH_3O_x}}{\mathrm{d}t} = \rho_{bed} \sum_{j=1}^{14} m_{ij} r_j\,. \tag{3}$$

The steady state concentrations of the intermediates calculated from the set of algebraic equations (1)–(3) were implemented into the differential equations of the C_2 and CO_x formation rates assuming an isothermally operated plug-flow reactor:

$$\frac{\mathrm{d}p_{C_2}}{\mathrm{d}(m_{cat}/F)} = k_7 (p_{CH_3})^2 - A\,, \tag{4}$$

List of symbols

a	external specific of the catalyst particle ($6\, d_p^{-1}\, \rho_{cat}^{-1}$)	r_j	rate of a reaction step (Pa ml g^{-1} s^{-1})
d_p	particle diameter (cm)	T	temperature (K)
F	flow rate (ml s^{-1})	t_{mod}	modified contact time = m_{cat}/F
k_j	rate constant (ml/(g s Pa^b))	m_{ij}	stoichiometric coefficient
k_g	mass transfer coefficient (cm s^{-1}) (correlation see Hougen et al. AIChE J., 8,5 (1962))	Θ_i	degree of surface coverage
		ρ_{bed}	density of catalyst bed (g ml^{-1})
		indices	
m_{cat}	weight of catalyst (g)	s	surface
p_i	partial pressure (Pa)	g	gas-phase
p_{total}	total pressure (Pa)		

$$\frac{\mathrm{d}p_{\mathrm{CO}_x}}{\mathrm{d}(m_{\mathrm{cat}}/F)} = B + C \tag{5}$$

with

$$\begin{aligned}
A &= 0 && \text{(models 1–4, 9, 10)},\\
&= r_{11} = k_{11}\Theta_{[\mathrm{O}_2]}p_{\mathrm{C_2H_6}} && \text{(models 5–8)},\\
B &= r_8 = k_8 p_{\mathrm{CH_3}}\Theta_{[\mathrm{O}]} && \text{(models 1–9)},\\
C &= 0 && \text{(model 1)},\\
&= r_9 = k_9\Theta_{\mathrm{O_2}}p_{\mathrm{CH_3}} && \text{(model 2)},\\
&= r_{10} = k_{10}p_{\mathrm{O_2}}p_{\mathrm{CH_3}} && \text{(model 3)},\\
&= r_2 = k_2\Theta_{[\mathrm{O}_2]}p_{\mathrm{CH_4}} && \text{(models 4, 10)},\\
&= r_{11} = 2k_{11}\Theta_{[\mathrm{O}_2]}p_{\mathrm{C_2H_6}} && \text{(models 5–8)}.
\end{aligned}$$

The kinetic data have been evaluated taking account for interparticle mass transfer limitations of oxygen, methyl radicals and ethane (see stationary balances in eqs. (6)–(8)):

$\mathrm{O_2}$: $k_{\mathrm{g}}a(p_{\mathrm{O_2,g}} - p_{\mathrm{O_2,s}}) = -\sum r_{j,\mathrm{s}}$

$(j = 3; 4$ (see reaction models table 1)); (6)

$\mathrm{CH_3}$: $k_{\mathrm{g}}a(p_{\mathrm{CH_3,g}} - p_{\mathrm{CH_3,s}}) = \sum r_{j,\mathrm{s}} - \sum \overline{r_j}$

$(j_{\mathrm{s}} = 1; 8; 9; j = 7, 10$ (see reaction models table 1)

with $\overline{p_{\mathrm{CH_3}}} = (p_{\mathrm{CH_3,s}} + p_{\mathrm{CH_3,g}})/2$ and $p_{\mathrm{CH_3,g}} \ll p_{\mathrm{CH_3,s}}$); (7)

$\mathrm{C_2H_6}$: $k_{\mathrm{g}}a(p_{\mathrm{C_2H_6,g}} - p_{\mathrm{C_2H_6,s}}) = \sum r_{j,\mathrm{s}} + k_7(\overline{p_{\mathrm{CH_3}}})^2$

$(j_{\mathrm{s}} = 11$ (see reaction models table 1)). (8)

Only the gas-phase concentrations of the reactants $\mathrm{CH_4}, \mathrm{O_2}$ and the products $\mathrm{C_2}$, CO_x were known. The surface and gas-phase intermediate concentrations Θ_i, $p_{\mathrm{CH_3O}_x}$ resulted from the feed concentration, the rate constants k_j were estimated by an optimization procedure summarized below.

The optimization criterion was the minimum of the sum of the relative deviations between measured and calculated data at constant temperature:

$$Q(\boldsymbol{k}) = \sum_{i=1}^{4}\sum_{n=1}^{n_{\mathrm{total}}}\left|\frac{p_{\mathrm{calc},i,n} - p_{\mathrm{exp},i,n}}{p_{\mathrm{exp},i,n}}\right| \times 100\% \tag{9}$$

(i denotes the reactants $\mathrm{CH_4}, \mathrm{O_2}, \mathrm{CO}_x, \mathrm{C_2}$; n is the total number of data points).

Parameters were estimated by a stochastic search algorithm ("genetic algorithm") [17,18] by which the global minimum of eq. (9) was found with high probability. This was of special interest since no a priori estimates of the parameters were available. Therefore a search within a parameter space covering initially a range of magnitude from 10^{-15} to 10^{30} was required. Solutions without physicochemical meaning, i.e. negative concentrations and surface coverages as well as $\Theta_i > 1$, were rejected. In one optimization 800 parameter vectors were generated on which 8000 further iterations were based. The quality of the parameters obtained was judged by repeating the procedure up to five times. A confidence measure of the estimated parameters was derived from their standard deviations based on the five optimization runs (cf. model 5 and table 2).

4. Results and discussion

4.1. MODEL DISCRIMINATION

The most significant criterion for the model discrimination was the capability of the different models to fit the reactor outlet partial pressure of ethane. The effect of the inlet oxygen partial pressure was of particular interest since the ethane partial pressure passed through a maximum as a function of $p^0_{O_2}$ for all catalysts containing CaO. The fit of the different models is illustrated for one catalyst (10 mol% CaO, $T = 933$ K) in fig. 2. The pattern of the experimental data was matched by model 5; this was valid for the total range of temperatures, partial pressures and catalyst compositions applied (cf. figs. 3a–3h). The consideration of CO_2 adsorption (models 6–8) did not improve the fit of experimental data. The quality of the various models is depicted in table 1 by the average relative error of all predicted data ($Q(k)/n_{total}$) as a function of the inlet partial pressure of CH_4 and O_2, temperature and catalyst composition.

Table 2
Standard deviations of the final parameter estimates (reaction model 5)

Rate constant k_j	Range of standard deviation for catalysts and temperatures applied (%)
k_1	25–32
k_{-1}	48–71
k_4	12–15
k_{-4}	30–36
k_5	35–44
k_6	26–33
k_7	8–11
k_8	8–13
k_{11}	12–16

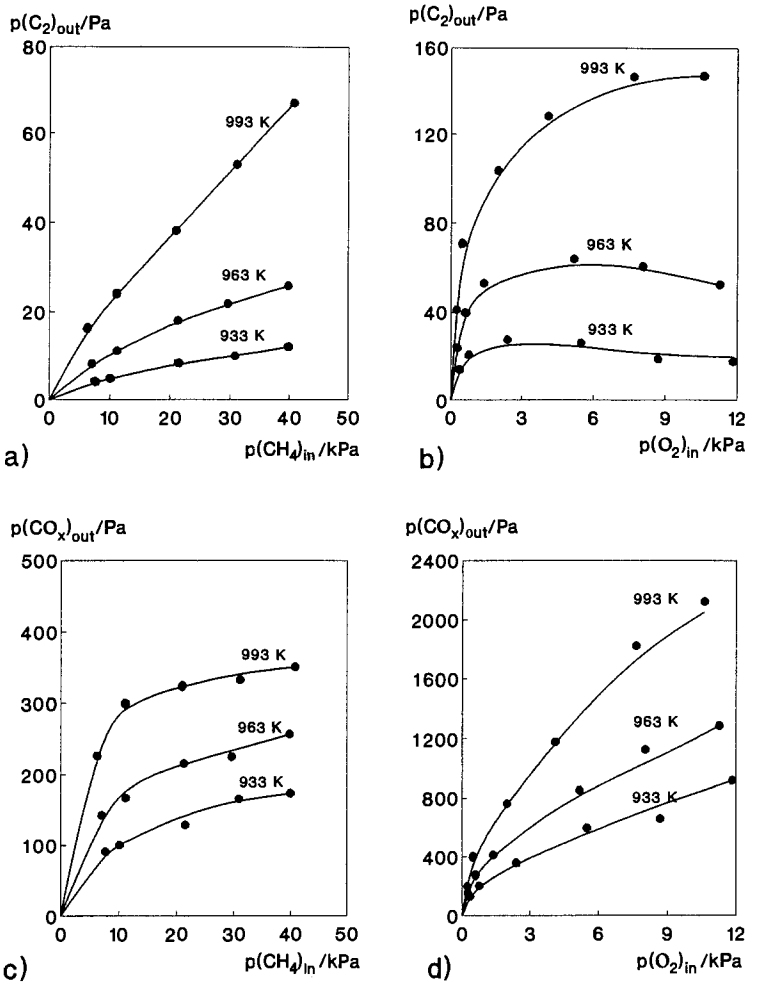

Fig. 3. C_2 and CO_x outlet partial pressure as the function of the oxygen and methane inlet partial pressure; (experimental data (points) and simulations of model 5 (lines)) catalysts: (a–d) 10 mol% CaO/CeO_2; (e–h) pure CeO_2.

4.2. KINETIC MODEL 5

According to model 5 (see table 1) methane is reversibly activated by monoatomic surface oxygen sites resulting in methyl radicals and surface OH-groups ($j = 1$). Gas-phase oxygen is incorporated into the surface via its molecular adsorption and consecutive dissociation. CH_3 species either react with monoatomic oxygen sites on the surface ($j = 8$) resulting in total oxidation or recombine in the gas-phase ($j = 7$). A second source of CO_x formation besides reaction $j = 8$ is the oxidation of ethane by molecular oxygen species on the surface ($j = 11$). This reaction leads to an accelerated consumption of ethane and a lowering of C_2 selectivity

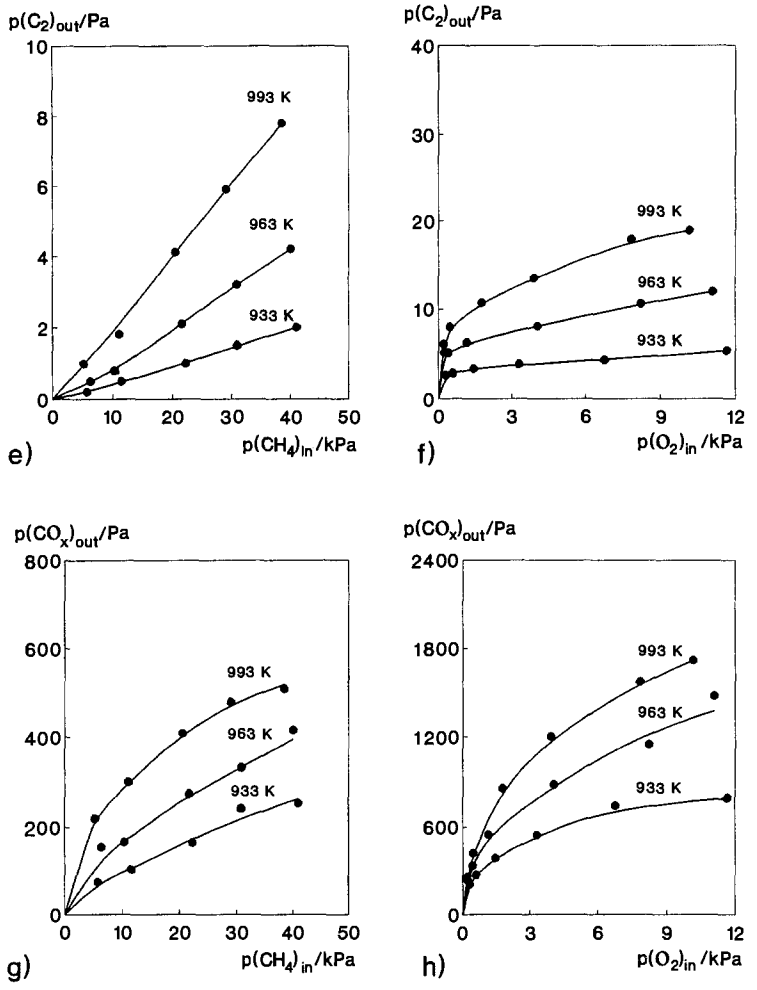

Fig. 3. (Continued).

with increasing oxygen partial pressure. Therefore the product distribution is likely controlled by the capability of catalysts to dissociate gas-phase oxygen and by the activity of the dissociated oxygen to oxidize CH_3.

4.3. RATE CONSTANTS AS FUNCTION OF CATALYST COMPOSITION

Constants obtained for the elementary steps of model 5 are compared with respect to catalyst composition in fig. 4.

Any interpretation of the temperature dependence of these rate constants is elusive resulting from the statistical uncertainties of the parameters (table 2), the narrow temperature range (60 K) chosen and the small number (3!) of different temperature levels. For these reasons no activation energies were determined.

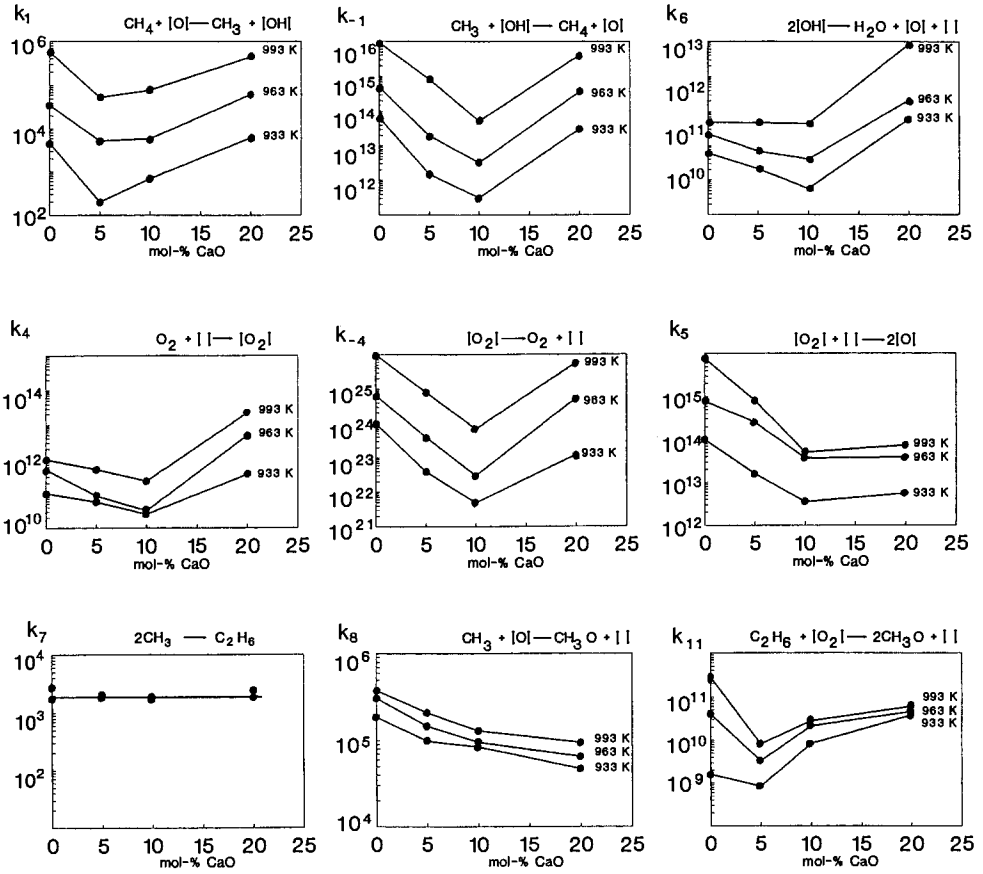

Fig. 4. Values of estimated parameters k_j (model 5) as the function of the catalyst composition. k_j in $(\mathrm{ml}/(\mathrm{g\,s\,Pa}^b))$: $b = -1$ if $j = -4, 5, 6$; $b = 0$ if $j = 1, -1, 4, 8, 11$; $b = 1$ if $j = 7$.

Nevertheless, the similar dependence of all rate constants for each temperature level on the catalyst composition supports the applicability of model 5.

4.3.1. Gas-phase reaction

The validity of the method of parameter estimation and partly also of model 5 itself is confirmed by the fact that the estimated rate constant k_{11} of the non-catalytic gas-phase reaction is independent both of catalyst composition and temperature within the range investigated [13]; its value when related to the gas phase volume (ca. 2.6×10^{13} $\mathrm{cm^3\ mol^{-1}\ s^{-1}}$) is in the same order of magnitude as known from literature sources (1.16×10^{13} $\mathrm{cm^3\ mol^{-1}\ s^{-1}}$) [13].

4.3.2. Catalytic reactions

Considering the dependencies of the rate constants on catalyst composition (fig. 4) relations between the electrical properties and the particular rate constants are evident (cf. fig. 1).

At this point it should be emphasized that a distinction between electronic states of the active surface sites, i.e. surface defects ($V_o^{\cdot\cdot}$, $V_o^{\cdot}$, V_o) and surface oxygen species (O^-, O^{2-} and O_2, O_2^-, O_2^{2-}) is not possible by the modelling procedure based on gas-phase kinetic data. Therefore, the rate constants of the catalytic reactions reflect a distribution of various electronic states and various reactivity of surface sites. For instance, n- and p-type conductors affect this distribution by providing electron donors or acceptors for the surface species. Furthermore, the oxygen anion conductivity is related to the number of surface oxygen defects [19,20]. In the following paragraphs the correlations between rate constants and electrical properties are discussed with due consideration of these aspects.

The dependence of the rate constant of the CH_3 formation ($j = 1$) and of its reverse reaction ($j = -1$) on catalyst composition (fig. 4) shows a minimum between a CaO content of 5 and 10 mol% in the catalyst. High absolute electron conductivity seems to promote the methane activation as is illustrated by the correlation between the rate constant k_1 and the overall electron conductivity of the catalysts (cf. fig. 1 and fig. 4). If both, n-type and p-type conductors promote methyl radical formation, the only requirement to the catalyst should be the availability of electron acceptors. Methane activation on n-type conductors (CeO_2) may be related to the reaction of lattice oxygen and the reduction of the reducible cation ($Ce^{4+} + e^- \rightarrow Ce^{3+}$) whereas in the case of p-type conductors the electron acceptors might be provided by positive holes ($h^+ + e^- \rightarrow 0$) [19,20]. However, electron donors required for the reverse reaction ($j = -1$) are supplied in the same manner.

The rate of oxygen adsorption ($j = 4$) is expected to depend on both, the type of electron conductivity and the oxygen-anion conductivity, the latter being related to the concentration of oxygen defect sites. However, the dependence obtained (fig. 4) points to a dominant influence of the p-type conductivity, providing a high concentration of electrons and a fast electron transfer to gas-phase oxygen (cf. fig. 1). The rate constant of oxygen desorption ($j = -4$) has a minimum at a catalyst composition of 10 mol% (fig. 4) that corresponds to the maximum of oxygen-ion conductivity at a CaO content of 10–15 mol% and is in the range of low electron conductivity (fig. 1). Thus, this reaction is promoted by a high electron mobility of the catalyst as well. The increase in the rate constant of oxygen dissociation ($j = 5$) with increasing n-type conductivity possibly results from a partial reduction of Ce in the steady state of the catalysts with Ce content and thus, from the high oxygen affinity of vacant sites.

Only sparse knowledge is available from literature about the reactivity of surface OH-groups. Therefore, the surface dehydration ($j = 6$) as a function of catalyst composition cannot be easily interpreted. This reaction includes splitting of different bonds: $[OH] \rightarrow [O] + H^{\#}$; $[OH] \rightarrow [\,] + OH^{\#}$; $H^{\#} + OH^{\#} \rightarrow H_2O$ (with # indicating some kind of an intermediate form). Hence, the reaction requires different properties of active sites which might be provided by doping CeO_2 with CaO.

The activity of monoatomic surface oxygen for the oxidation of CH_3 radicals ($j = 8$) decreases monotonously with increasing CaO content as well as with

decreasing n-type and or increasing p-type conductivity (fig. 1). The observed correlation between electron conductivity and reducibility of cations with the solids on the one hand and catalytic performance on the other hand agrees with results of Lunsford et al. [11], who found a dependence between the activity of lattice oxygen for the oxidation of CH_3 radicals and the reducibility of different oxide catalysts. Since in reaction $j = 11$, i.e. the consecutive oxidation of ethane by molecular surface oxygen sites, several reaction steps are lumped, no dependence of the global reaction rate constant k_{11} on particular catalyst properties can be derived. Nevertheless, there appears to be an influence of the electron conductivity.

4.4. SIMULATION

As a sensitivity characteristic of the overall reaction rate to the rate of individual steps the integral selectivity to ethane at complete oxygen conversion was chosen. The estimated rate constants of the most selective catalyst containing 20 mol% CaO in the solid solution was decreased or increased by one order of magnitude (see table 3). Hereby it should become evident which rates affect mainly total com-

Table 3
Change of C_2-selectivity by decreasing (−) and increasing (+) rate constants for the 20 mol% CaO/CeO_2 catalyst by one order of magnitude ($p^0_{CH_4} = 90$ kPa, $p^0_{O_2} = 10$ kPa, $T = 993$ K)

Rate constant k_j [a]	Δk_j	t_{mod} (g s ml^{-1}) ($x_{O_2} > 99.9\%$)	S_{C_2} (%)	$\frac{S^+_{C_2} - S^-_{C_2}}{\log(k^+) - \log(k^-)}$ [b]
as estimated [a]		0.32	14.4	–
k_1	−	0.125	5.1	20.1
	+	0.031	45.3	
k_{-1}	−	0.031	45.3	−20.1
	+	0.125	5.1	
k_4	−	0.305	30.4	−10.5
	+	0.018	9.3	
k_{-4}	−	0.018	9.3	10.5
	+	0.305	30.4	
k_5	−	0.230	7.5	9.5
	+	0.025	26.5	
k_6	−	0.087	10.0	10.5
	+	0.046	31.0	
k_7 [c]	−	0.086	2.5	25.9
	+	0.023	58.5	
k_8	−	0.073	43.2	−19.0
	+	0.061	5.2	
k_{11}	−	0.076	36.5	−16.2
	+	0.055	4.1	

[a] As estimated, see fig. 4.
[b] Sensitivity measure of the selectivity influenced by the particular rate constants.
[c] Fictitious simulation since k_8 is no surface rate constant.

bustion and ethane formation. Simulations based on model 5 were carried out for $p_{CH_4} = 90$ kPa, $p_{O_2} = 10$ kPa and $T = 993$ K; the contact time was chosen in such a way that O_2 was completely converted. From table 3 it can be derived that every rate constant of the proposed reactions influences the selectivity.

Increasing the rate of methyl radical formation (reaction $j = 1$) increases C_2 selectivity strongly; as shown above it can be affected by high electron conductivity (n-type as well as p-type). An increase in the reverse reaction rate ($j = -1$) leads to an opposite change in selectivity. The methyl radical oxidation ($j = 8$) by which the C_2 selectivity is diminished can be suppressed by avoiding n-type conductivity. The acceleration of the surface dehydration ($j = 6$) leads to increase in ethane selectivity because new oxygen defects are created. Consequently, dissociation of diatomic oxygen is promoted and total combustion of ethane by diatomic oxygen is suppressed. The rate constants of reactions $j = 4, -4, 5$ and 11 should be discussed in the same context. If total oxidation is to be avoided, the adsorption of diatomic surface oxygen ($j = 4$) should be slow and reactions of diatomic oxygen ($j = -4, 5$) should be fast to suppress any diatomic oxygen on the surface. There are two possibilities to realize these requirements. First, a catalyst is to be provided with n-type conductivity. Secondly and more reasonably, a p-type conductor should be used because the oxidation of methyl radicals is avoided simultaneously. It should be noted that these are fictitious considerations since most of rate constants, such as k_1 and k_{-1}, k_4, k_{-4} and k_5, are interrelated via solid properties and cannot be controlled independently.

5. Conclusion

The derivation of rate constants estimated for schemes of elementary reactions by a stochastic search algorithm on the one hand and of relationships between solid state properties, reaction conditions and the selectivity of various catalysts on the other hand has been proven to be useful. From the correlations between surface rate constants and the electrical properties of the $CaO–CeO_2$ catalysts the conclusion is drawn that electron acceptors and donors play a major role in the reactions. Reactions leading to methyl radicals and subsequently to ethane as well as to their total combustion are obviously coupled via solid-state properties. These findings would explain the limits of the ethane and / or ethylene yield as discussed for the oxidative coupling of methane [16].

Based on the results described above non-steady state operation of a catalytic reactor looks beneficial for improving C_2 hydrocarbon yield by suppressing high diatomic oxygen concentration on the surface. Furthermore, rate constants for the elementary surface reactions would support the optimization of reactor design as was recently suggested by Iglesia et al. [21].

Acknowledgement

The author expresses her gratitude to Professor Manfred Baerns, Ruhr-University Bochum, for his continuous encouragement and many stimulating discussions while this work was carried out.

References

[1] O.V. Krylov, Catal. Today 18 (3) (1993).
[2] E.E. Wolf, ed., *Methane Conversion by Oxidative Processes*, Van Nostrand Reinhold Catalysis Series (Van Nostrand Reinhold, New York, 1992).
[3] J.A. Dumesic, D.F. Rudd, L.M. Aparicio, J.E. Rekoske and A.A. Trevino, in: *The Microkinetics of Heterogeneous Catalysis*, ACS Professional Reference Book (Am. Chem. Soc., Washington, 1993).
[4] V.H. Möbius, Z. Chem. 4 (1964) 81.
[5] R.M. Blumenthal, F.S. Bruguer and J.E. Garnier, J. Electrochem. Soc. 120 (1973) 1230.
[6] D. Wolf, B. Ferrand and G. Gayko, unpublished.
[7] M. Kemna, Diploma Thesis, Bochum, Germany (1992).
[8] D.-J. Driscoll and J.H. Lunsford, J. Phys. Chem. 89 (1985) 4415.
[9] Y. Feng, J. Niirama and D. Gutman, J. Phys. Chem. 95 (1991) 6558, 6564.
[10] O.V. Buyevskaya, M. Rothaemel, H.W. Zanthoff and M. Baerns, J. Catal. 146 (1994) 346.
[11] Y. Tong and J.H. Lunsford, J. Am. Chem. Soc. 113 (1991) 4741.
[12] D.J. Driscoll, W. Martir, X.J. Wang and J.H. Lunsford, J. Am. Chem. Soc. 107 (1985) 58.
[13] J. Warnatz, in: *Combustion Chemistry*, ed. W.C. Garnier (Springer, Berlin, 1984).
[14] R.A. Cox, in: *Modern Gas Kinetics – Theory, Experiment and Application*, eds. M.J. Pilling and I.W. Smith (Blackwell, Sci. Publ., Oxford, 1987) p. 262.
[15] F. Freund, G.L. Maiti, F. Battlo and M. Baerns, J. Chim. Phys. 87 (1990) 1467.
[16] A. Shamsi, Ind. Eng. Chem. Res. 32 (1993) 1877.
[17] R. Moros, Computer programme Gendgls, University Leipzig, Germany (1992).
[18] D.E. Goldberg, in: *Genetic Algorithm in Search, Optimization & Machine Learning* (Addison Wesley, Reading, MA, 1989).
[19] A. Bielanski and J. Haber, in: *Oxygen in Catalysis* (Dekker, New York, 1991).
[20] J.-L. Dubois and C.J. Cameron, Appl. Catal. 67 (1990) 49.
[21] S.C. Reyes, C.P. Kelkar and E. Iglesia, Catal. Lett. 19 (1993) 167.